The collapse of cooperation during range expansion of *Pseudomonas aeruginosa*

Nan Luo[#1,6], **Jia Lu**[#1], **Emrah Şimşek**[#1], **Anita Silver**[1], **Yi Yao**[1], **Xiaoyi Ouyang**[2], **Stuart A. West**[3], **Lingchong You**[1,4,5,*]

[1]Department of Biomedical Engineering, Duke University, Durham, NC 27708, USA

[2]School of Physics, Peking University, Beijing, China

[3]Department of Biology, University of Oxford, Oxford, UK

[4]Center for Quantitative Biodesign, Duke University, Durham, NC 27708, USA

[5]Department of Molecular Genetics and Microbiology, Duke University School of Medicine, Durham, NC 27708, USA

[#] These authors contributed equally to this work.

Abstract

Cooperation is commonly believed to be favorable in spatially structured environments, as these systems promote genetic relatedness that reduces the likelihood of exploitation by cheaters. Here, we show that a *Pseudomonas aeruginosa* population that exhibited cooperative swarming was invaded by cheaters when subjected to experimental evolution through cycles of range expansion on solid media, but not in well-mixed liquid cultures. Our results suggest that cooperation is disfavored in a more structured environment, which is the opposite of the prevailing view. We show that spatial expansion of the population prolongs cooperative swarming, which was vulnerable to cheating. Our findings reveal a mechanism by which spatial structures can suppress cooperation through modulation of the quantitative traits of cooperation, a process that leads to population divergence towards distinct colonization strategies.

Introduction

Cooperation is one of the most essential and ubiquitous social relationships across biological populations and communities, including single-celled microbes [1]. Cooperative

[*]Corresponding author. Department of Biomedical Engineering, Duke University, CIEMAS 1381, 101 Science Drive, Box 3382, Durham, NC 27708, USA., Tel.: +1 (919)660-8408; Fax: +1 (919)668-0795; you@duke.edu.
[6]Present address: Shenzhen Institute of Advanced Technology, Chinese Academy of Sciences, Shenzhen, China

AUthor Contributions

N. L. conceived the research, designed and performed modeling and experiments, interpreted the results, and wrote the manuscript. J. L. and E. Ş. Designed and performed experiments, interpreted the results, and assisted with manuscript revisions. A. S. assisted with modeling, results interpretation, and manuscript revisions. Y. Y. assisted with experiments. X. O. assisted with modeling and experiments. S. W. assisted with results interpretation and manuscript revisions. L.Y. conceived the research, assisted in research design, interpreted the results, and wrote the manuscript.

Conflict of Interest

The authors declare no competing interests.

Europe PMC Funders Author Manuscripts

communities can potentially be invaded by cheaters: non-cooperative individuals that reap the benefits of cooperation without contributing [2]. Understanding the evolutionary dynamics between cooperators and cheaters is key to explaining the existence of cooperation and the evolution of complex cooperative societies [3]. Extensive theoretical and experimental studies suggested that spatial structures tend to maintain cooperation and resist cheating [4–11]. Hamilton showed that cooperation is favored when the donor and recipient of the cooperative behavior are genetically related, because the benefits of cooperation will be preferentially directed towards related cooperators and less accessible to cheaters [12–15]. In spatially structured systems with limited dispersal, cooperators and cheaters can self-organize into clusters, and such spatial assortment increases the genetic relatedness between interacting individuals and maintains cooperation [4, 9, 10, 16–18].

The degree to which an individual cooperates could also depend upon the spatial structure of a system. Many cooperative traits in microbial populations, for example, are regulated by environmental factors, such as the availability of resources [19–23] or the presence of quorum-sensing signals [24–26]. As such, spatial structure can lead to heterogeneity of those environmental factors which can, in turn, impact the evolutionary dynamics of cooperative traits through modulation of cell physiology, *in addition to or instead of causing spatial assortment*. This alternative role of spatial structure has been largely overlooked in previous theoretical analyses, which normally assume that the cooperating or cheating trait of an individual is fixed in either spatially structured environments or well-mixed ones.

Here we show a unique suppression of cooperation by spatial dynamics through experimental evolution of a bacterial population that relies on cooperative swarming. We found that the cooperative ancestral population was invaded by cheaters during cycles of range expansion on solid media but not under well-mixed conditions. We demonstrated that the spatial structure of the growth environment alters the availability of the nutrients, leading to longer periods of cooperation. Hence our findings reveal that spatial dynamics drive the collapse of cooperation by altering the physiological state of cells.

Results

Experimental evolution led to a population fitness decline

Colonies of *Pseudomonas aeruginosa* PA14 developed long and sparse branches on solid swarming media [21]. We subjected PA14 to experimental evolution by serial passaging: after 20 hours of growth, each colony was collected, and ~10^6 cells were center inoculated onto a fresh plate (Fig. 1a). After repeating the procedure for eight consecutive days, patterns of colonies changed substantially in all four independent lineages initiated from the same ancestral strain (Fig. 1b). Meanwhile, population fitness, defined as the total biomass accumulation of the colony, declined over the course of evolution (Fig. 1c, Extended Data Fig. 1).

We isolated 100 clones from the evolved population of Lineage 1 for phenotypic and genetic analysis (Fig. 2a, Fig. S1). When mixed with equal cell density, these 100 isolates reconstituted the colony pattern of the evolved population (Fig. 2b). Therefore, we consider the collection of these isolates to be a good proxy for the evolved population. The clonal

population of each isolate was characterized by its total area and branching index (the ratio between the colony circumference and the circumference of a circle of equal area). The branching index is minimized to 1 in circular colonies and increases with the development of branches. Based on these two characteristics, the colony patterns of these isolates fell into three categories (Fig. 2c, d): wildtype-like colonies (16%) that developed long and thin branches; hyperswarmers (43%) that developed circular or irregular colonies that covered the entire plate, similarly to those previously reported [27]; and nonswarmers (41%) that developed very short or no branches. Across the categories, the number of colony-forming units (CFUs) were similarly proportional to biomass accumulation (Fig. S2). Therefore, we continued to measure population fitness in biomass accumulation below.

Whole genome sequencing of 95 isolates identified a total of 18 unique genetic variations, nine of which did not cause significant changes in the colony patterns (Fig. 2c, Fig. S3, Table S1). Among the 38 nonswarmers, 33 harbor mutations in either *lasR* or *rsaL*, which encode quorum sensing regulators that are involved in rhamnolipids production [28–32]. The selection of multiple alleles that led to the same nonswarming phenotype indicates that this trait has a significant competitive advantage during evolution. All 41 hyperswarmers harbor a single point mutation (V178G) in *fleN*, which encodes a flagellar synthesis regulator. Van Ditmarsch et al. have discovered that this mutation confers on bacterial cells multiple polar flagella and hyperswarming [27]. Most wildtype-like isolates and five nonswarmers carry none of these 18 mutations but may carry intergenic mutations or variations not identified by sequencing due to low coverage.

We observed distinct evolutionary outcomes when the same ancestral strain was evolved in a well-mixed liquid medium, which differs from the swarming medium only in the absence of agar. Evolved liquid cultures exhibited a slight increase in the growth rate and yield (Extended Data Fig. 2a), but there was no apparent change in the colony patterns of the evolved populations or their isolates (Extended Data Fig. 2b, c). This absence of a phenotypic change is not explained by a difference in the total number of generations for the liquid vs. the agar media (Supplementary Note 1). Therefore, evolution on a solid agar surface uniquely selects mutants which reduce population fitness and alter the colony swarming phenotype.

Divergent evolution yielded three colonization strategies

The distinct colony patterns of the three types of strains indicate their differences in swarming, which is the major form of cell movement when dense colonies of *Pseudomonas* spread over solid agar media [33]. Bacterial swarming requires individual-level features such as flagella and multicellular behavior such as the production of surfactants [34–36]. In *P. aeruginosa*, the synthesis of rhamnolipids, a major type of biosurfactants, is regulated by a quorum sensing cascade, LasI/LasR and RhlI/RhlR systems [20, 29]. RsaL acts as a negative regulator of quorum sensing by binding to the *lasI* promoter [31, 32]. Quorum sensing mutants *lasI*- and *rhlI*- are defective in rhamnolipids biosynthesis and swarming [21]. Therefore, the nonswarmers with mutations in *lasR* or *rsaL* we identified may also be impaired in surfactant production. Indeed, surfactants produced by nonswarmers were

undetectable using the established drop collapse assay [37] and significantly lower compared to those produced by wildtype (Extended Data Fig. 3).

We examined pairwise interactions between strains by inoculating fluorescently labelled strains next to each other (fluorescent labeling did not change the relative magnitudes of growth rates between the strains; Fig. S4). Nonswarmers were immotile on their own but swarmed along with wildtype or hyperswarmers (Fig. 3a, Fig. S5), as observed with the *rhlA*$^{-}$ mutant that lacks rhamnolipids biosynthesis [21, 38]. This observation suggests that biosurfactants are public goods that facilitate the collective movement of cells.

Previous studies reported that *Pseudomonas* resisted the invasion of *rhlA*$^{-}$, which had no significant growth advantage over wildtype [21, 26]. However, the nonswarmers we identified (mutated in *lasR* or *rsaL*) showed a 4% increase in growth rates (Fig. 3b, Fig. S6), possibly due to a lower metabolic burden with impaired quorum sensing. Nonswarmers benefit from the public goods produced by swarmers without making contributions; therefore, they are “cheaters” that exploit the cooperative behavior of others (nonswarmers will hereafter be called “cheaters”). The emergence and dominance of these cheaters during evolution demonstrates that cooperative swarming can be susceptible to cheating.

Hyperswarmers synthesized extra flagella that promote their swimming motility but reduce their growth [27]. Consistently, we found hyperswarmers grew slower than the wildtype (Fig. 3b). Hyperswarmers also carried along cheaters during colony expansion, yet they spread faster than the other strains when mixed (Fig. 3a, Fig. S5), suggesting that the additional motility they gained was non-cooperative.

In a nutshell, the characterization of the strains isolated from experimental evolution suggests the emergence of three distinct colonization strategies on a solid medium: investment in either surfactant-facilitated cooperative motility, flagella-dependent non-cooperative motility, or individual-level proliferation (Fig. 3c). Strains that excel in one aspect are less capable in the other two, indicating a trade-off between different strategies due to resource limitation [39].

Multi-strain spatial patterns constrain colony growth model

The cooperative ancestral populations of *P. aeruginosa* were invaded by cheaters and hyperswarmers only on solid plates but not in well-mixed liquid cultures. Spatial assortment has been proposed to shape cooperative populations with spatial structures [4, 9, 10, 16–18]. However, in multi-strain colonies, we did not observe spatial segregation between strains or cell clusters of one strain that excluded others (Fig. S7). Strains were labelled with either RFP or YFP due to strong cyan and green autofluorescence in *P. aeruginosa* [40]. For three-strain colonies, we labelled two strains at a time.

Cooperative trait itself may also be influenced by spatial structures. However, experimental observation of the spatial-temporal dynamics of the cooperative trait is challenging. Therefore, we sought to develop a model to elucidate population dynamics within multi-strain colonies on a solid surface with a diffusive nutrient (Methods, Table S3). As proposed above, the expansion of each coexisting strain depends on growth and two sources of

motility: autonomous motility that is independent of other strains, and cooperative motility that is contributed by all coexisting strains. Based on the physiological characterizations, the three types of strains differ in each associated parameter (Fig. 3c). To constrain the relative contributions of each element in the model, we observed the spatial distributions of strains in multi-strain colonies by fluorescent imaging (Fig. 4a, Fig. S7). As found in the hitchhiking experiments (Fig. 3a), with wildtype alone, cheaters traveled as far as wildtype, but with hyperswarmers, they were slower and absent from the colony front (Fig. S7). Observed spatial distributions of cheater-hyperswarmer colonies constrained the relative contributions of autonomous and cooperative motilities (Fig. S8). In three-strain colonies, cheaters expanded faster than wildtype (Fig. 4a), indicating that growth also contributed significantly to bacterial range expansion when cells were mobile.

Our model was based on a coarse-grained modeling framework for branching colonies we had previously developed [41]. In this model, the colony morphology development was simplified as branch formation and growth. The branch width and density of each strain are pre-determined parameters, and those of a multi-strain colony were calculated from the population composition. Each branch extended following the local nutrient gradient. The branches of each strain extended at a rate proportional to the growth and motilities of that strain.

Previous models often assumed a homogenous growth environment and a constant level of the cooperative trait [4, 5, 42–45], while we considered the heterogeneity of nutrient distribution during colony expansion and the dependence of the cooperative trait on nutrient availability. Rhamnolipid biosynthesis in *Pseudomonas* is triggered by nitrogen limitation but restrained under prolonged starvation as a form of metabolic prudence [20, 21]. Our measurements also showed that surfactant production by wildtype and hyperswarmers was highest at intermediate nutrient levels (Extended Data Fig. 4). Consistently, the growth advantage of cheaters over wildtype and hyperswarmers was the most significant under this condition (Fig. S9). Therefore, we describe the cooperative motility of cells by a nutrient-dependent box function (Methods): cells exhibit cooperative motility and a reduced growth rate only within an intermediate range of nutrient concentration. The model does not take mutation into consideration, and all simulations are deterministic.

Our model captures a high-level picture of how strains interact during range expansion: the expansion of cheaters is facilitated by other strains, and the presence of cheaters compromises population fitness as measured by biomass accumulation (Fig. 4b). Consistent with experiments, simulations showed that colonies with cheaters accumulated less biomass than those without. Notably, hyperswarmers partially rescued the biomass reduction in three-strain colonies, as shown by the increased biomass of three-strain colonies compared to wildtype-cheater colonies (Fig. 4b, Extended Data Fig. 5).

Advantage of cheaters depended on growth environments

To understand the cause of the observed evolutionary divergence on solid media, we investigated how these strains would compete and the spatial-temporal dynamics of cooperative motility during the competition.

In experiments, we mixed fluorescently labeled strains in varying ratios and grew them either on solid plates or in liquid media. The final composition of the population was determined after 18 hours of growth. In well-mixed liquid co-cultures with wildtype, cheaters only showed a small increase in the relative abundance (Fig. 5a, Extended Data Fig. 6a). In contrast, on a solid medium, cheaters were significantly more competitive than wildtype, especially when their initial fraction was low (Fig. 5a, Extended Data Fig. 6a). This result explains their emergence during evolution on solid plates. Consistently, our model also showed that cheaters became more competitive than wildtype during colony expansion on solid media than during liquid growth (Fig. 5a, Extended Data Fig. 6a).

Modeling revealed that the increased cheating on solid surfaces originated from the spatial heterogeneity of nutrients and the nutrient-dependence of the cooperative trait. In a liquid culture, the nutrient concentration was uniform and decreased monotonically over time (Fig. 5b). Since cooperative motility is induced within a certain range of nutrient concentration, there was only a limited time window when the cooperators would sacrifice their individual growth (Fig. 5b). In contrast, on a solid medium, the nutrient distribution became heterogeneous. Over a prolonged timeframe, the balance between consumption of nutrients and expansion into new nutrient-rich territories continuously maintained the nutrient concentration at the colony front within the range in which cooperation occurs (Fig. 5c). The resulting prolonged cooperation allowed colonies to expand efficiently, but also made them more vulnerable to cheating. These results are consistent with a recent study, which showed that the expression of *rhlAB* (rhamnolipids biosynthesis operon) in *P. aeruginosa* raised within a much narrower range of growth rate during liquid growth than on solid plates [26].

Consistent with previous experimental studies [27], our model showed that on solid media, wildtype was outcompeted by hyperswarmers (Extended Data Fig. 6b), which had a higher autonomous motility. However, the advantage of hyperswarmers was lost in liquid environments where motility is dispensable (Extended Data Fig. 6b).

In addition, modeling showed that increasing the growth rate or the autonomous motility are two alternative strategies for a variant to outcompete the wildtype during swarming (Fig. S10). When cheaters and hyperswarmers grew together on a solid medium, however, they exhibited a negative frequency-dependent selection, in which each strain outcompeted the other when initially at a low frequency (Extended Data Fig. 6c, turquoise). This observation indicates that the enhanced selfish (private) form of motility rescued hyperswarmers from exploitation by cheaters. The competition between cheaters and hyperswarmers reflects a trade-off between growth and motility in an expanding colony [39]. The coexistence between fast-growing and fast moving subpopulations during colonization [39] could be the result of such a trade-off.

Evolutionary outcomes depended on nutrient availability

The competitive advantage of cheaters and hyperswarmers in spatially structured environments explains their invasion during colony expansion of *Pseudomonas*. Modeling showed that, when populations were subjected to multiple rounds of spatial expansion and bottlenecking, wildtype was invaded by cheater and hyperswarmer and eventually driven

out (Fig. 6a, middle panels). Cheater and hyperswarmer would coexist afterwards (Fig. 6a, middle panels).

As demonstrated above, the evolution of cheating in *Pseudomonas* is associated with the spatial structure of the growth environment because of the dependency of cooperation on nutrient availability. Therefore, manipulating the initial nutrient concentration should alter the evolutionary outcomes of *Pseudomonas* during spatial expansion. Indeed, modeling predicted that the cheater fraction expanded only at an intermediate nutrient concentration (Fig. 6a), which maximized the cooperative swarming trait but also rendered the cooperators exploitable. Meanwhile, the hyperswarmer invaded at low and intermediate nutrient levels, where autonomous motility was a major driver to colony expansion (Fig. 6a). Under nutrient-rich conditions, wildtype was much more resistant to both strains (Fig. 6a). The evolutionary outcomes may vary with different initial mutant fractions or stochastic mutation events.

These predictions were corroborated by experimental evolution on solid media with varying amounts of nutrients (Fig. 6b, Fig. S11). Again, we isolated strains from each evolved population and analyzed the morphology of their colonies (Fig. 6c). Each new isolate was categorized by determining whether its morphology falls within the 95% confidence interval of the probability distributions of each group (Fig. 2c, contour lines). The analysis revealed that intermediate nutrient levels led to the divergence of the population into three phenotypic groups, whereas low nutrient availability resulted in the dominance of hyperswarming strains, and a high nutrient level sustained the wildtype population (Fig. 6c). Additional experimental evolution was conducted to show that these distinct outcomes did not result from the difference in the total generation numbers under each condition (Supplementary Note 1, Fig. S12). These findings indicate that evolutionary outcomes are dependent on growth environments, and thus explain the discrepancy between our results and a previous study using the same ancestral strain and similar protocols which always yielded hyperswarmers but no cheaters [27].

Discussion

Growth in a spatially extended environment is commonly assumed to promote the maintenance of cooperation, because spatial structure can allow the assortment of cooperators and cheaters [4, 6, 9, 18]. Here, however, we demonstrate that spatial structures caused by growing on a solid surface can also disfavor cooperation. *P. aeruginosa* cells produce biosurfactant as a public good, and this trait is exploited by cheaters only during range expansion on solid surfaces but not in well-mixed liquid cultures. In this system, we did not observe spatial clustering of cooperators on solid surfaces. In fact, during the evolution experiment, the spatial information of a population was erased when cells were reseeded to a new plate. Therefore, the effect of spatial structure on population clustering (relatedness) is not responsible for the observed evolutionary dynamics.

In contrast, we found that growing on solid surface favors cheating because it leads to different levels of cooperation. Biosurfactant production in *P. aeruginosa* is nutrient dependent, so the heterogeneity and overall availability of the nutrient in a spatially

structured system lead to distinct dynamics of this trait. Our model shows that, on solid media, the combination of colony expansion and nutrient consumption creates an environment that induces continuous biosurfactant production, which in turn drives colony expansion. This feedback loop results in a prolonged period (higher level) of cooperation, which creates a vulnerability to cheating. On the other hand, in a well-mixed liquid system, the nutrient level is spatially homogenous and monotonically decreases over time, leaving a limited time window in which cooperation is possible. This difference indicates that spatial structures may directly impact cell physiology and thereby alter the evolutionary dynamics of cooperation. That is, the emergence of the cheaters is not due to the spatial structure per se, but due to higher expression of the cooperative traits in a spatially extended environment.

The cooperative trait in our system − biosurfactant production − is critical for the efficient dispersal of *Pseudomonas* cells on solid surfaces. To maximize its efficacy, this trait is under tight regulation linked to external conditions to ensure that cooperation is “turned on” when it is the most beneficial: during the spatial expansion of a colony. But a mechanism that optimizes cooperation for greater population fitness does not necessarily help with maintaining cooperation. The spatial heterogeneity during colony growth triggers cooperation, but as a side effect it allows for the invasion of cheaters. In that regard, this mechanism is a high-risk, high-reward strategy at the population level. Quorum sensing is another such strategy: quorum sensing regulates cooperation to ensure that it is cost-effective [46], but quorum sensing mutants are widespread in nature [47, 48].

Apart from the invasion of cheaters, we also observed the emergence of hyperswarmers in our system. Compared to surfactant production, hyperswarmers invest more on flagella synthesis [27], which confers a relatively private benefit. This strategy mitigates exploitation by cheaters while preserving the cooperative trait. Therefore, hyperswarming can be regarded as a partial-privatization strategy to resist cheating, analogous to that found with iron acquisition of *P. aeruginosa* [49, 50].

Hyperswarmers and cheaters eventually reach a dynamic coexistence, leading to a divergence of the original population. Diversification in microbial communities is common in nature [51–53]. Factors accounting for such diversification include spatial heterogeneity that creates niches, increased mutation rate, and horizontal gene transfer [51]. Here, we show that social conflict gives rise to divergent evolution in an initially cooperative population, resulting in coexisting strains with distinct survival strategies.

Methods

Bacterial strains and growth conditions

We used *Pseudomonas aeruginosa* PA14 as the wildtype and the ancestral strain in experimental evolution. To grow bacterial colonies and observe patterns, bacteria were cultured in LB medium overnight in a shaker incubator at 37°C and 200 rpm. The overnight culture (200 μl) was diluted in 1 ml fresh LB medium and incubated at 37°C and 200 rpm for an additional 3 hours to allow the cells to recover to the exponential growth stage and reach a final concentration of OD_{600} 0.2 to 0.4. The swarming medium was freshly prepared [21], and 20 ml of medium was pipetted into each petri dish (100 mm, Falcon). After the

medium had solidified, 1 μl of cell culture was pipetted onto the medium surface at the center of each plate, and plates were left to dry on the bench for 15 min with lids open. The plates were then incubated upside down at 37°C in an incubator.

Swarming medium

We prepared swarming medium to generate branching patterns of *P. aeruginosa* according to the following recipe adapted from [21]: 200 ml of 5x stock phosphate buffer, 1 ml of 1 M $MgSO_4$, 1 ml of 0.1 M $CaCl_2$, casamino acids stock solution (200 g/L), agar stock solution (1.25%, melted), and sterilized water to make up 1 liter. The volumes of casamino acids and agar were determined by the required final concentrations. To make 1L 5x phosphate buffer stock solution, we dissolved 12 g Na_2HPO_4 (anhydrous), 15 g KH_2PO_4 (anhydrous), and 2.5 g NaCl in water and sterilized by autoclaving. To make 200 ml casamino acids stock solution, we dissolved 40 g casamino acids (Gibco™ Bacto™ 223120) in water and sterilized by filtering. To make 1L agar stock solution, we added 12.5 g granulated agar (BD Difco™ 214530) in water and sterilized by autoclaving. Each swarming plate was prepared by pipetting exactly 20 ml of medium into a petri dish (100 mm, Falcon), and the dish was allowed to cool for 20 min to 1 hour.

Experimental evolution and sequencing

We carried out experimental evolution of *P. aeruginosa* PA14 on swarming media with 8 g/L casamino acids (unless indicated otherwise) and 0.5% agar. After 20 hours of growth, we collected the entire colony from the plate by flushing cells off with 1.5 ml LB medium. The biomass was determined by measuring OD_{600}. We used approximately 10^6 cells to inoculate a new plate with swarming medium. This procedure was repeated for seven consecutive days. As the control group, overnight cultures of the ancestral strain were repeatedly seeded to the same type of medium each day. The evolved population of day 7 was streaked on a LB plate to isolate individual strains that emerged during evolution.

Genomes of the isolates and the ancestral strain were sequenced using Illumina NovaSeq (6000 S-prime 150 bp PE) with an average of 300-400 coverage. Initial read quality checks were carried out using FastQC. Sequencing reads were then processed using the TrimGalore toolkit to trim low-quality bases from the 3’ end of the reads and Illumina sequencing adapters. Only reads that were 20 nt or longer after trimming were kept for further analysis. Reads were aligned to the Ensembl *P. aeruginosa* PA14 genome reference (Pseu_aeru_PA14_V1) using BWA-mem. Putative variants were detected using variant caller FreeBayes and annotated. Only variants for which at least one sample had been genotyped as different from the reference were kept.

Growth curve measurement

We measured the growth curves of *P. aeruginosa* using a plate reader (Tecan Infinite 200). In each well of a 96-well plate, we added 200 μl liquid media (with the same composition with swarming media but without agar) and 2 μl cell culture (overnight cultures of different replicates and strains were diluted 10× ~ 50× to the same cell density). To prevent evaporation, we either added 50 μl mineral oil to each well (Fig. 3b, Fig. S4, and Fig. S9) or used Nunc Edge multi-well plates (Thermo Scientific) with built-in water

reservoirs (Fig. S6). The cells were then incubated in the plate reader at 37°C, and OD_{600} measurements were taken at 10-min intervals for 24 hours. Background signals measured from media containing no cells were subtracted from the data. For replicates of a particular strain, cells of the same stock were inoculated into different wells of a 96-well plate and measured.

Drop collapse assay

We used a protocol previously established for assessing biosurfactant production by *P. aeruginosa* with minor modifications [37]. Cells from the overnight cultures were inoculated in 3 ml of liquid media (with the same composition with swarming media but without agar) to an initial OD_{600} = 0.0016. After 20 h at 37°C and 225 rpm, OD_{600} of the cultures were measured. Supernatants were obtained by filtering (0.22 μm polyethersulfone; VWR) and diluted by a factor proportional to the OD_{600}. For each diluted supernatant, 25 μl was dropped on a polystyrene (hydrophobic) 96-well plate lid. After two minutes at room temperature, the area of each droplet was measured and normalized by the droplet area of the negative control (blank media), leading to the normalized droplet area. The experiment was run twice independently. In each run, for each sample a total of 18 replicates were run and averaged.

Competition assay

Overnight cultures of each competing strain with fluorescent labeling were revived, centrifuged, resuspended in fresh LB, and diluted to the same OD_{600}. The cultures of each strain were mixed in varying ratios. Approximately $3x10^6$ cells were inoculated onto fresh swarming plates or into liquid swarming media (replicates of the same initial ratio were inoculated separately). After 18 hours of growth at 37°C, cells were collected from plates or liquid media, and plated on LB after serial dilution to allow colony counting. On the next day, colonies on the LB plates were imaged under a fluorescent microscope to determine the colony count of each strain.

Imaging

Bacterial colonies growing on plates were imaged with a UVP Colony Doc-It Imaging Station with epi white light. The brightness and contrast of all images were enhanced using the same setting. Fluorescent imaging was performed with a Keyence BZ-X710 fluorescence microscope and Keyence BZX Software Suite 1.3.1.1. To image a swarming colony, the entire plate was scanned, and the images were stitched together using the built-in algorithm of the microscope. All fluorescent images were color-coded in the same scheme for consistency (magenta for wildtype or wildtype-like strains, yellow for nonswarmers, and cyan for hyperswarmers). Images were analyzed with ImageJ 1.53k.

Mathematical modeling

Model formulation

The model is formulated based on the coarse-grained framework for branching colony growth we developed in the previous work [41]. The model considers the spatial-temporal dynamics of nutrient within the medium and the cell density of each coexisting strain

within the colony. The shape of the colony is determined by preset parameters to avoid mechanistic details of pattern formation in this system. We develop the model with minimal assumptions that captures the key elements of colony growth: cell growth (multiplication), cell movement, nutrient consumption, and nutrient diffusion.

The colony composes of n strains ($n = 3$ in this study). The cell density of the kth strain is $C_k(\mathbf{x}, t)$, ($k = 1, 2, \ldots, n$), which is a function of the position ($\mathbf{x}$) and time (t). Each strain has different parameters, including α_k (cell growth rate), h_k (cooperative motility coefficient), g_k (autonomous motility coefficient), and r_k (response coefficient to cooperative motility). As in our previous model [41], we consider colony patterns and the spatial-temporal dynamics of cells as two separate variables. The pattern of a colony defines its boundary, and within this boundary, cells grow (replicate) and migrate. For multi-strain colonies, we compute the pattern and cell density of each strain separately: each strain develops its own pattern, which defines the boundary within which the cells of this strain grow and migrate.

The computing process composes of three parts:

1 Pattern formation—When a colony is initiated from a single point inoculum at the center of a plate, it develops branches that extend and bifurcate as the colony expands.

In a single-strain colony, the branching pattern is characterized by two pre-defined parameters: branch width (W) and branch density (D, the number of branches in one unit of length). The growth directions of each branch follow the local nutrient gradient. The extension rate of a branch is determined by the motility of the population (see below). The local branch density of a branch is given by $\frac{1}{d}$, where d is the distance of the branch tip to its nearest neighbor; the branch bifurcates to maintain the local branch density around D. Specifically, we track the tip of a growing branch and calculate the local branch density. As the branch extends, if the local branch density falls below a predefined threshold, branch bifurcation is triggered and a new subbranch initiates. Because the local branch density doubles after a bifurcation event, the threshold branch density for bifurcation we choose is $\frac{2}{3}D$, so that the local branch density oscillates between $\frac{2}{3}D$ and $\frac{4}{3}D$. The total range covered by all branches of the colony is Ω, and the tip range of the ith branch is Ω_i', which is defined as a circle centered at the branch tip with a diameter of W.

In a multi-strain colony, each strain has its own set of branches. The branch width and density at the tip of the ith branch of the kth strain, W_{ik} and D_{ik}, are given by the weighted averages of the pre-defined branch widths and densities of single-strain colony patterns (W_k and D_k), weighted by the local fraction of each strain. Branches of different strains are initially overlapping. The growth direction of a branch of the leading strain (the strain with the fastest extending branches) follows the local nutrient gradient, while the ith branch of other strains follow the ith branch of the leading strain. The bifurcation of branches is determined in the same way as in the single-strain case.

The total expansion area of the ith branch of the kth strain is the product of the branch extension rate $\left(\frac{\mathrm{d}L_{ik}}{\mathrm{d}t}\right)$ and the branch width (W_{ik}). In the meantime, the total expansion area is

contributed by the cooperative and the autonomous motility of the *k*th strain. Therefore, we have

$$\frac{\mathrm{d}L_{ik}}{\mathrm{d}t}W_{ik} = g_k + r_k\sum_j\left(\int_{\Omega_{ik}^t} H_jG_j dx\right)$$

Here, g_k is the autonomous motility of the *k*th strain, and the second term on the right-hand side represents the cooperative motility. The cooperative motility contributed by the *j*th strain is proportional to $H_j(\boldsymbol{x}, t)$, the cooperative motility coefficient, and $G_j(\boldsymbol{x}, t)$, the cell growth of the *j*th strain (see below) within the *i*th branch tip of the *k*th strain. The magnitude of each strain's response to cooperative factors in its environment is expressed by the coefficient r_k. Hence, we have

$$\frac{\mathrm{d}L_{ik}}{\mathrm{d}t} = \frac{1}{W_{ik}}\left[g_k + r_k\sum_j\left(\int_{\Omega_{ik}^t} H_jG_j dx\right)\right] \quad (1)$$

Cooperative swarming of bacterial cells occurs when the nutrient concentration, $N(\boldsymbol{x}, t)$, is at an intermediate level, as described by the following step functions:

$$H_k = \begin{cases} 0, & N < N_a or N > N_b \\ h_k, & N_a \le N \le N_b \end{cases} \quad (2)$$

$$A_k = \begin{cases} \alpha_{max}, & N < N_a or N > N_b \\ \alpha_k, & N_a \le N \le N_b \end{cases} \quad (3)$$

where N_a and N_b are the lower and upper bounds of nutrient concentration that allows for cooperative swarming. Within this range, the cooperative motility coefficient H_k increases from 0 to h_k (the basal cooperative motility coefficient of the *k*th strain), and the growth rate A_k reduces from α_{max} (the maximum growth rate) to α_k (the basal growth rate of the *k*th strain).

2 Cell density distribution—The cell growth of the *k*th strain depends on the growth rate, the nutrient concentration, and the cell carrying capacity:

$$G_k = A_k\frac{N}{N + K_N}\left(1 - \frac{\sum_k C_k}{C_{max}}\right)C_k \quad (4)$$

Here, $C_k(\boldsymbol{x}, t)$ is the cell density distribution of the *k*th strain, K_N is the half-saturation nutrient concentration for nutrient-dependent cell growth, and C_{max} is the cell carrying capacity.

The total new biomass of the kth strain, $\int_{\Omega k} G_k dx$ (the amount of cell growth integrated over the pattern of the kth strain, Ω_k), is reallocated within the colony boundary of the kth strain proportionally to the remaining carrying capacity, $C_{max} - \sum_k C_k$, at each location, normalized by the total remaining capacity in the colony, $\int_{\Omega k} (C_{\max} - \Sigma_k C_k) dx$

$$\frac{\partial C_k}{\partial t} = \frac{C_{\max} - \Sigma_k C_k}{\int_{\Omega k} (C_{\max} - \Sigma_k C_k) dx} \int_{\Omega k} G_k dx \tag{5}$$

3 Nutrient distribution—The distribution of nutrient, $N(\boldsymbol{x}, t)$, is described by

$$\frac{\partial N}{\partial t} = D_N \nabla^2 N - \beta_N \sum_k G_k \tag{6}$$

where D_N is the nutrient diffusivity, and β_N is the consumption rate of nutrient.

The initial nutrient concentration is uniform and given by N_0. Patterns are initialized as a small circle at the center of the domain with a radius of r_0. The initial cell density $C = \frac{c_0}{2\pi r_0^2}$. The initial number of branch tips is $2\pi r_0 D$. Cells are growing in a square petri dish of side L. We enforce no-flux boundary conditions for the nutrient. Cells grow for a time period of T.

Simulation and parameter fitting

Parameter values for the model were selected through a two-stage screening process. In the first stage, a coarse screening of 20,000 possible parameter combinations was performed by selecting random parameter values from a uniform distribution between the minimum and maximum reasonable values. Simulations were performed for the same set of strain ratios for all parameter combinations: equal ratios of all possible subsets of strains being present, as well as simulations of communities containing wildtype and either 1% cheater or 10% cheater, to evaluate the dynamics of cheating mutations arising in a population.

Promising parameter values were automatically selected from the simulation results according to the following criteria from the observed experimental data. First, the biomass of a colony with all 3 strains must be less than the biomass of a wildtype colony. Second, when wildtype and hyperswarmer are grown together, hyperswarmer must grow out to a larger radius than wildtype. Third, when wildtype and cheater are grown together, wildtype must grow to a larger radius than cheater. Fourth, when all three strains are grown together, hyperswarmer should grow to the largest radius, followed by cheaters, with wildtype remaining within the smallest radius. Fifth, when cheater is introduced to the wildtype population at a low starting fraction, it should proliferate by outcompeting wildtype cells. In addition to these hard criteria, secondary criteria regarding the qualitative aspects of the

results, specifically colony area and strain competition ratios, were maximized. Following this automated analysis, seven reasonable parameter sets from the coarse-grained screen were identified for further investigation.

In the second stage of the parameter screening process, two rounds of local search were performed. In the first round, 2000 parameter values generated by introducing random perturbations of up to 20% to the best coarse-grained candidates were tested. The second round followed the same procedure as the first round, except that the starting parameter values were the best candidates from the first round of screening instead of those from the coarse screening. The optimal set of parameters (Table S3) obtained from the two-stage screening was used in all following simulations. Simulations with different parameter values were run in parallel on the Duke Compute Cluster.

Extended Data

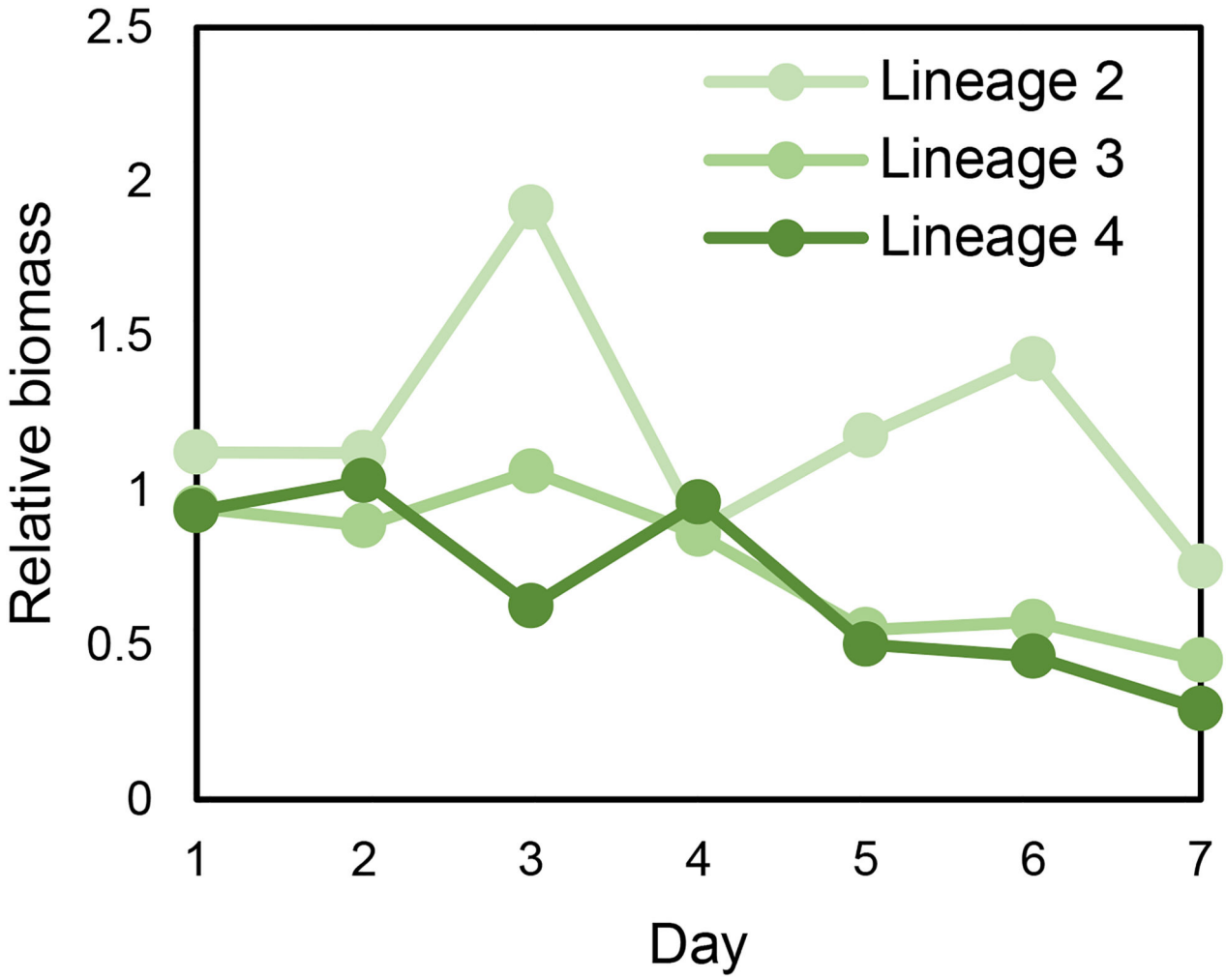

Extended Data Fig. 1. Experimental evolution of *P. aeruginosa* led to biomass decline.

The total accumulation of biomass of *P. aeruginosa* PA14 colonies declined during experimental evolution. Cells of a colony were flushed off the plate after colony growth for 20 h and resuspended, and the biomass was determined by measuring OD_{600}. The relative biomass of a colony was normalized by the average of wildtype colonies.

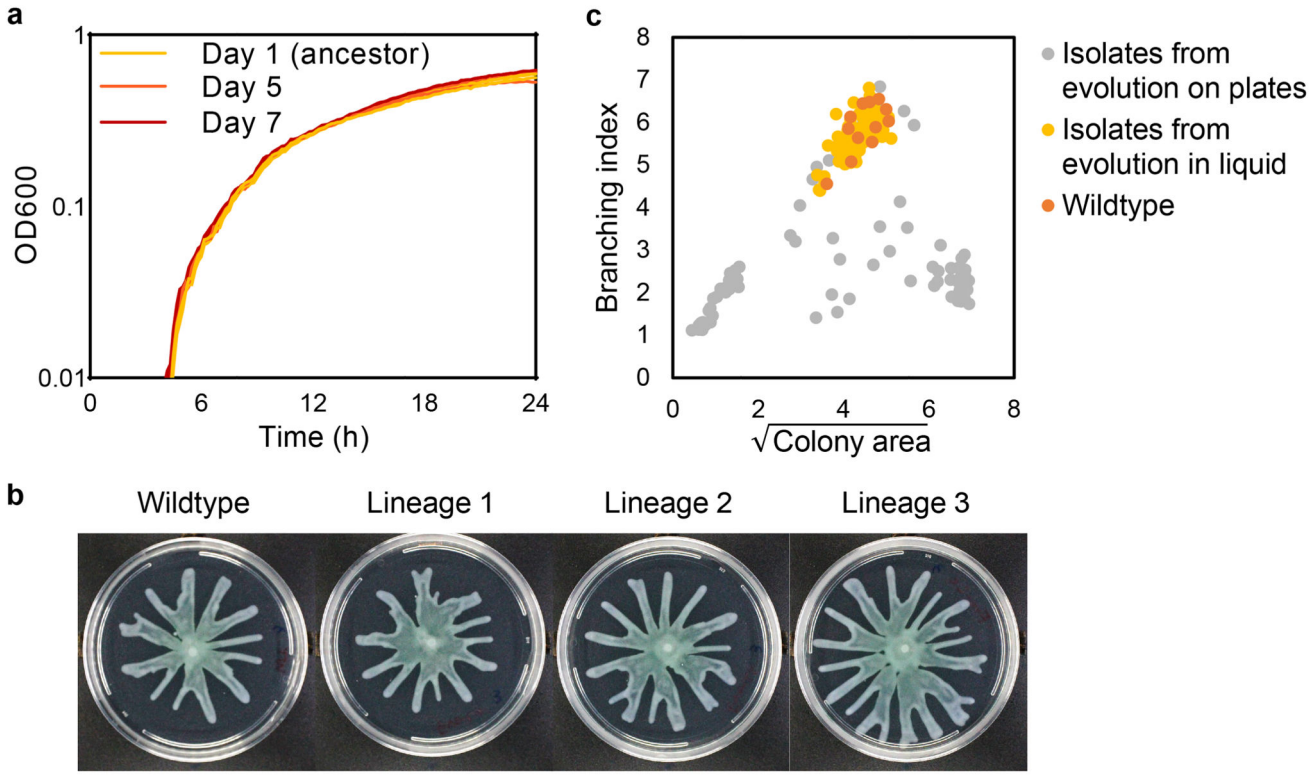

Extended Data Fig. 2. Nonswarmer or hyperswarmer did not emerge during experimental evolution of *P. aeruginosa* in liquid cultures.

a, The growth rate of *P. aeruginosa* increased during experimental evolution within liquid cultures. Growth curves were measured using cell cultures of the ancestral strain (Day 1) and the populations on Day 5 and Day 7 of the experimental evolution (n = 3 for each group; all replicates were shown). Both experimental evolution and the growth curve measurements were carried out using liquid swarming media with 8 g/L casamino acids.

b, Experimental evolution in liquid cultures did not alter the colony phenotype of *P. aeruginosa* or cause biomass decline. Shown are colonies of wildtype and the evolved populations of three independent lineages.

c, Comparison of the phenotypic characterizations of wildtype and isolates from populations evolved in liquid or on plates. Strains with nonswarming phenotype (low colony area with low branching index) or hyperswarming phenotype (high colony area with low branching index) did not emerge during evolution in liquid cultures.

Europe PMC Funders Author Manuscripts

Europe PMC Funders Author Manuscripts

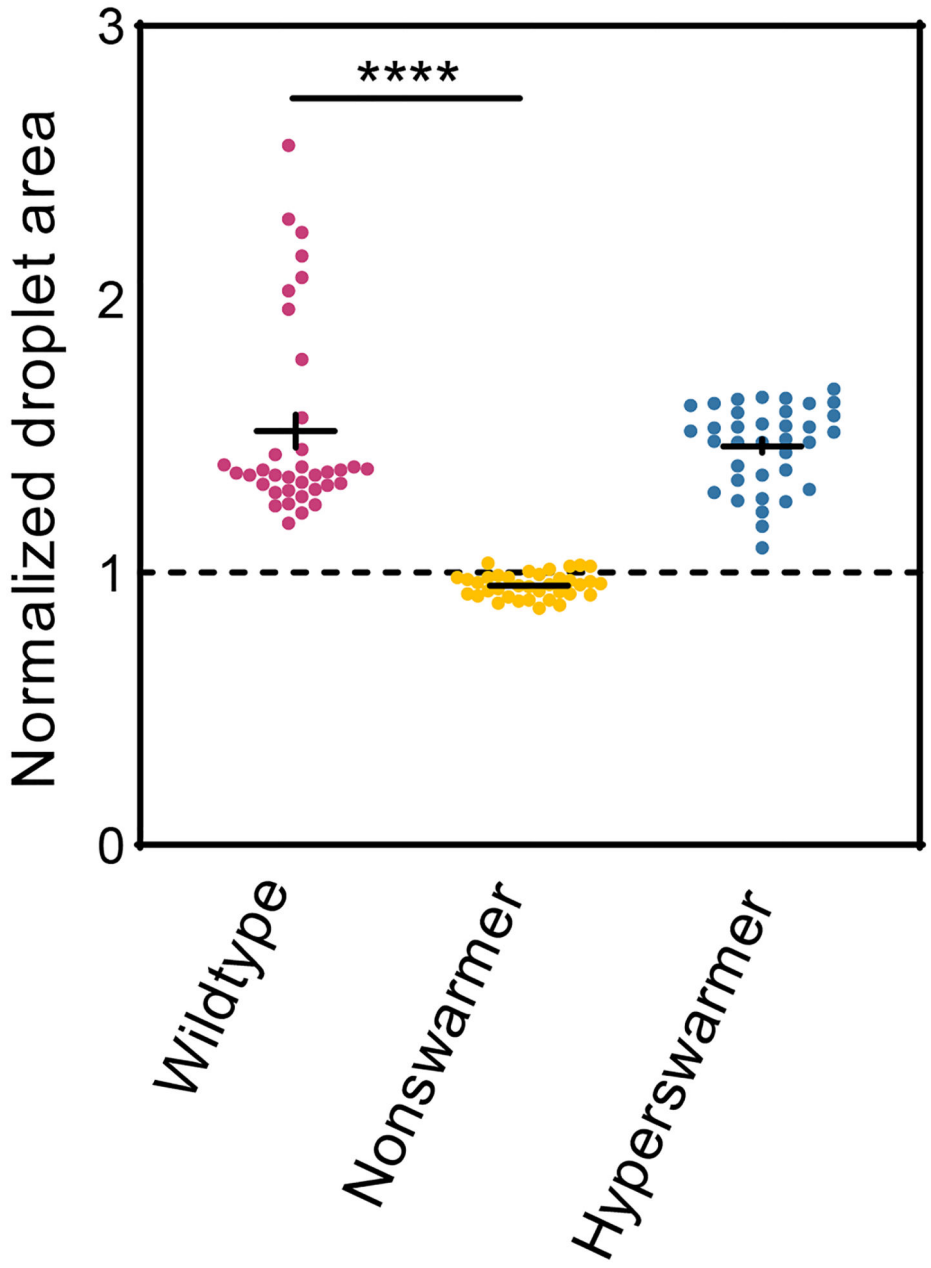

Extended Data Fig. 3. Nonswarmers are defective in surfactant production.

Cells were grown in liquid swarming media with 8 g/L casamino acids for 20 hours. The amount of surfactant in the supernatant was determined using the drop collapse assay. The droplet area (normalized by the negative control, blank medium) reflects the surfactant concentration. N = 36 for each group. Data are presented as mean values +/-SEM. Unpaired, two-sided *t* test with Welch's correction and a 95% confidence interval was used to compare between wildtype and nonswarmer. **** $P < 0.0001$.

Europe PMC Funders Author Manuscripts

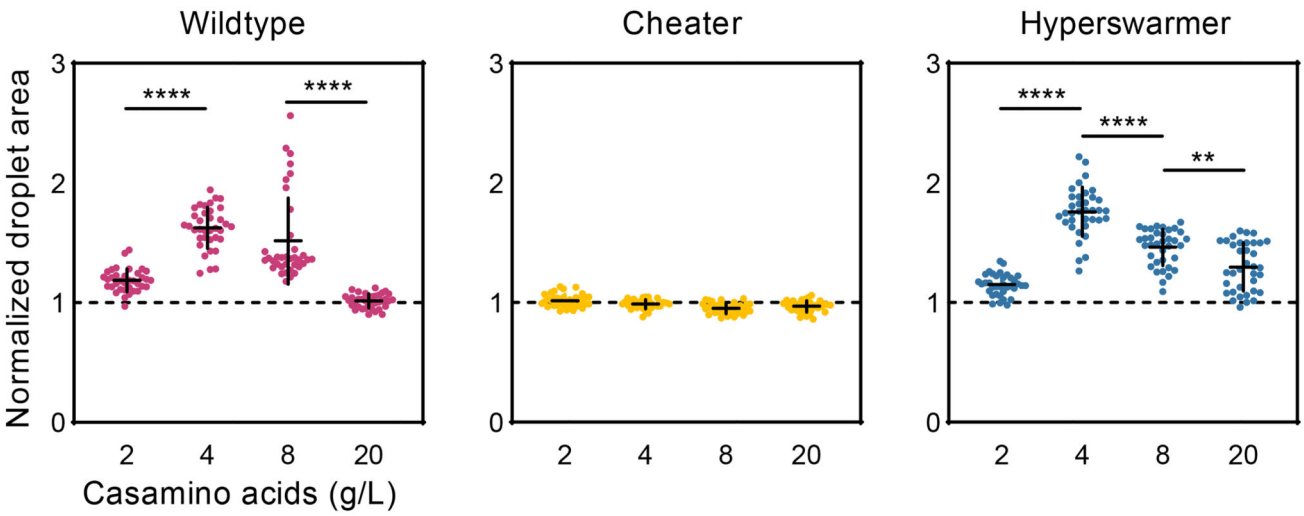

Extended Data Fig. 4. Intermediate nutrient level causes *P. aeruginosa* wildtype and hyperswarmers to produce the highest amount of surfactant.

Cells were grown in liquid swarming media with varying initial concentrations of casamino acids for 20 hours. The amount of surfactant in the supernatant was determined using the drop collapse assay. The droplet area (normalized by the negative control, blank medium) reflects the surfactant concentration. N = 36 for each group. Data are presented as mean values +/-SEM. Brown-Forsythe and Welch ANOVA test (which does not assume equal variances) were used to compare between groups. **** $P < 0.0001$, ** $P = 0.0014$. Data in Extended Data Fig. 3 were reused for comparison.

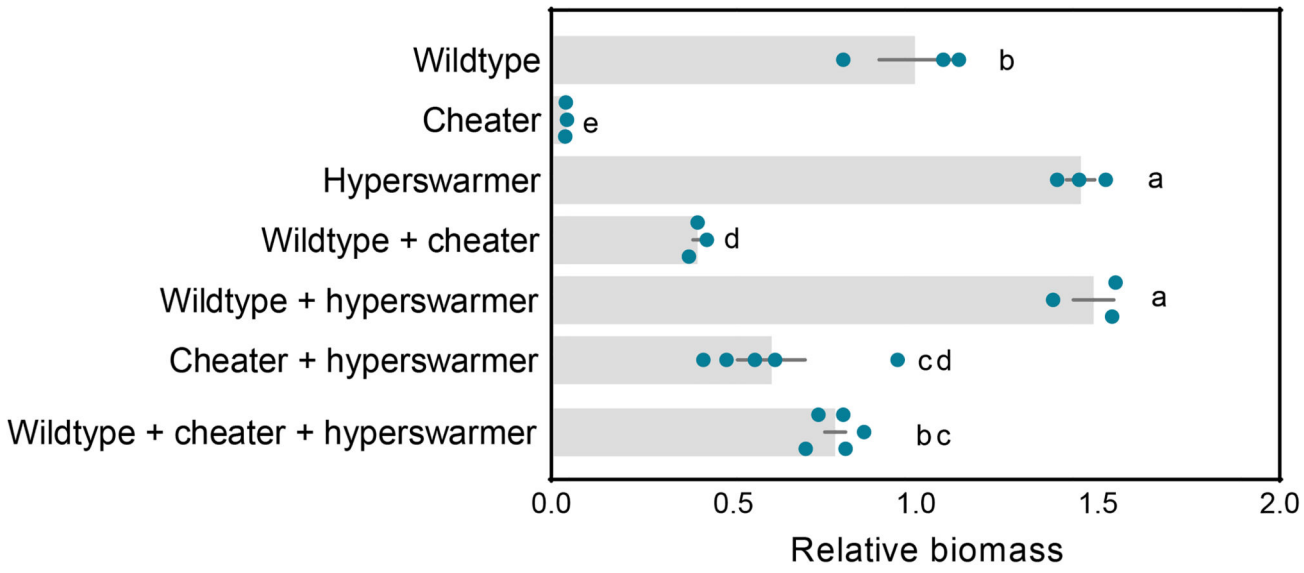

Extended Data Fig. 5. Cheater reduced the biomass accumulation of multi-strain colonies.

The total biomass of colonies with different compositions (normalized by wildtype) was determined by measuring OD_{600}. All data points were shown: n = 3-5 for each colony

type. Data are presented as mean values +/-SEM. One-way ANOVA followed by Tukey's multiple comparisons test (95% confidence intervals) was used to compare between groups. Significantly different groups are indicated by letters: groups with at least one common letter are not significantly different; otherwise, they are significantly different.

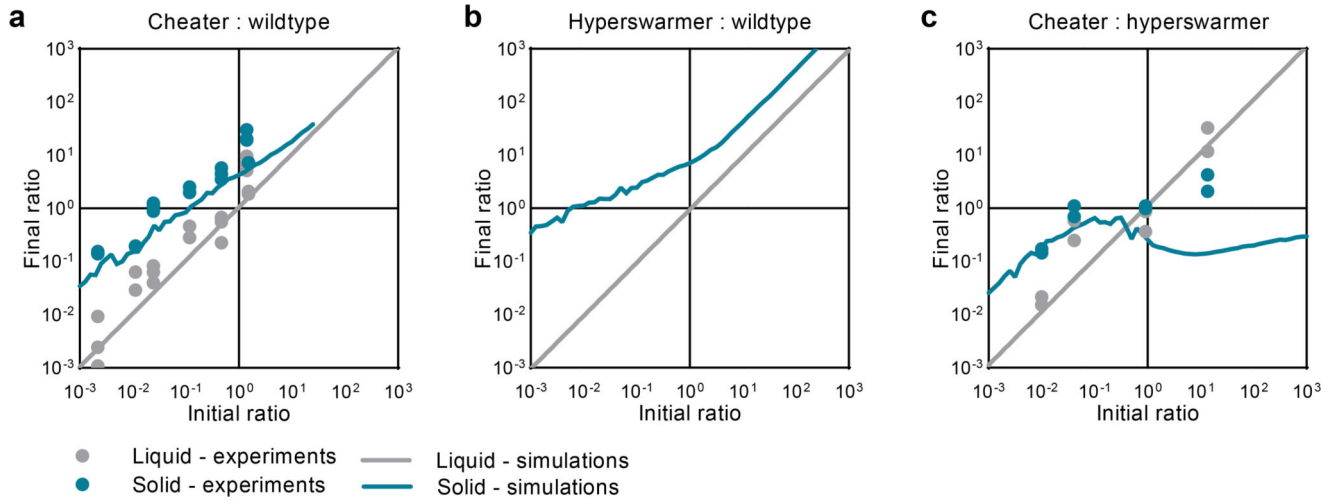

Extended Data Fig. 6. Model recaptured the competition dynamics between strains.
Pairwise competition between the three types of strains were carried out either in liquid cultures or on solid swarming plates. Competing strains with fluorescent labels were mixed in varying ratios and grown for 16 hours. The final population compositions were determined by CFU counting. In simulations, identical parameters were used when comparing liquid and solid phases. Data in panel **a** was presented in Fig. 4a in a different format.

Supplementary Material

Refer to Web version on PubMed Central for supplementary material.

Acknowledgements

We thank Duke Compute Cluster for assistance with high-throughput computation. We thank Joao Xavier (Memorial Sloan Kettering Cancer Center) for sharing *Pseudomonas aeruginosa* PA14 strains. This work was partially supported by grants from Office of Naval Research (LY: N00014-12-1-0631), National Science Foundation (LY: MCB-1937259), and National Institutes of Health (LY: R01GM098642).

Data Availability

The data that support the findings of this study are available on Zenodo: https://doi.org/10.5281/zenodo.10210659. Raw sequencing reads from whole genome sequencing are deposited in the NCBI Sequence Read Archive (BioProject PRJNA875393).

Europe PMC Funders Author Manuscripts

Europe PMC Funders Author Manuscripts

Code availability

The MATLAB codes used for data generation and/or analysis in the study are available on GitHub: https://github.com/youlab/MultistrainPatterns_NanLuo.

References

1. Celiker H, Gore J. Cellular cooperation: insights from microbes. Trends Cell Biol. 2013; 23: 9–15. [PubMed: 22999189]
2. Ghoul M, Griffin AS, West SA. Toward an evolutionary definition of cheating. Evolution. 2014; 68: 318–31. [PubMed: 24131102]
3. West SA, Cooper GA, Ghoul MB, Griffin AS. Ten recent insights for our understanding of cooperation. Nature ecology & evolution. 2021; 5: 419–430. [PubMed: 33510431]
4. Nowak MA, May RM. Evolutionary Games and Spatial Chaos. Nature. 1992; 359: 826–829.
5. Nowak, MA, Sigmund, K. Games on Grids, in The Geometry of Ecological Interactions: Simplifying Spatial Complexity. Metz, JAJ, Law, R, Dieckmann, U, editors. Cambridge: Cambridge University Press; 2000. 135–150.
6. Ackermann M, Stecher B, Freed NE, Songhet P, Hardt WD, Doebeli M. Self-destructive cooperation mediated by phenotypic noise. Nature. 2008; 454: 987–90. [PubMed: 18719588]
7. Funk F, Hauert C. Directed migration shapes cooperation in spatial ecological public goods games. PLoS Comput Biol. 2019; 15 e1006948 [PubMed: 31393867]
8. Xavier JB, Foster KR. Cooperation and conflict in microbial biofilms. Proc Natl Acad Sci U S A. 2007; 104: 876–81. [PubMed: 17210916]
9. Momeni B, Waite AJ, Shou W. Spatial self-organization favors heterotypic cooperation over cheating. Elife. 2013; 2 e00960 [PubMed: 24220506]
10. Hol FJ, Galajda P, Nagy K, Woolthuis RG, Dekker C, Keymer JE. Spatial structure facilitates cooperation in a social dilemma: empirical evidence from a bacterial community. PLoS One. 2013; 8 e77042 [PubMed: 24167557]
11. Xu S, Van Dyken JD. Microbial expansion-collision dynamics promote cooperation and coexistence on surfaces. Evolution. 2018; 72: 153–169. [PubMed: 29134631]
12. Hamilton WD. The genetical evolution of social behaviour. I. J Theor Biol. 1964; 7: 1–16. [PubMed: 5875341]
13. Hamilton WD. The genetical evolution of social behaviour. II. J Theor Biol. 1964; 7: 17–52. [PubMed: 5875340]
14. Griffin AS, West SA, Buckling A. Cooperation and competition in pathogenic bacteria. Nature. 2004; 430: 1024–7. [PubMed: 15329720]
15. Nowak MA. Five rules for the evolution of cooperation. Science. 2006; 314: 1560–3. [PubMed: 17158317]
16. West SA, Griffin AS, Gardner A. Evolutionary explanations for cooperation. Curr Biol. 2007; 17: R661–72. [PubMed: 17714660]
17. Cornwallis CK, West SA, Griffin AS. Routes to indirect fitness in cooperatively breeding vertebrates: kin discrimination and limited dispersal. J Evol Biol. 2009; 22: 2445–57. [PubMed: 19824927]
18. Lion S, Baalen M. Self-structuring in spatial evolutionary ecology. Ecol Lett. 2008; 11: 277–95. [PubMed: 18070102]
19. Sexton DJ, Schuster M. Nutrient limitation determines the fitness of cheaters in bacterial siderophore cooperation. Nat Commun. 2017; 8 230 [PubMed: 28794499]
20. Boyle KE, Monaco H, van Ditmarsch D, Deforet M, Xavier JB. Integration of Metabolic and Quorum Sensing Signals Governing the Decision to Cooperate in a Bacterial Social Trait. PLOS Computational Biology. 2015; 11 e1004279 [PubMed: 26102206]
21. Xavier JB, Kim W, Foster KR. A molecular mechanism that stabilizes cooperative secretions in Pseudomonas aeruginosa. Mol Microbiol. 2011; 79: 166–79. [PubMed: 21166901]

22. Kummerli R, Jiricny N, Clarke LS, West SA, Griffin AS. Phenotypic plasticity of a cooperative behaviour in bacteria. J Evol Biol. 2009; 22: 589–98. [PubMed: 19170825]
23. Butaite E, Kramer J, Wyder S, Kummerli R. Environmental determinants of pyoverdine production, exploitation and competition in natural Pseudomonas communities. Environ Microbiol. 2018; 20: 3629–3642. [PubMed: 30003663]
24. Diggle SP, Griffin AS, Campbell GS, West SA. Cooperation and conflict in quorum-sensing bacterial populations. Nature. 2007; 450: 411–4. [PubMed: 18004383]
25. Sandoz KM, Mitzimberg SM, Schuster M. Social cheating in Pseudomonas aeruginosa quorum sensing. Proc Natl Acad Sci U S A. 2007; 104: 15876–81. [PubMed: 17898171]
26. Monaco H, Liu KS, Sereno T, Deforet M, Taylor BP, Chen Y, Reagor CC, Xavier JB. Spatial-temporal dynamics of a microbial cooperative behavior resistant to cheating. Nat Commun. 2022; 13 721 [PubMed: 35132084]
27. van Ditmarsch D, Boyle KE, Sakhtah H, Oyler JE, Nadell CD, Deziel E, Dietrich LE, Xavier JB. Convergent evolution of hyperswarming leads to impaired biofilm formation in pathogenic bacteria. Cell Rep. 2013; 4: 697–708. [PubMed: 23954787]
28. Latifi A, Foglino M, Tanaka K, Williams P, Lazdunski A. A hierarchical quorum-sensing cascade in Pseudomonas aeruginosa links the transcriptional activators LasR and RhIR (VsmR) to expression of the stationary-phase sigma factor RpoS. Mol Microbiol. 1996; 21: 1137–46. [PubMed: 8898383]
29. Pesci EC, Pearson JP, Seed PC, Iglewski BH. Regulation of las and rhl quorum sensing in Pseudomonas aeruginosa. J Bacteriol. 1997; 179: 3127–32. [PubMed: 9150205]
30. Ochsner UA, Fiechter A, Reiser J. Isolation, characterization, and expression in Escherichia coli of the Pseudomonas aeruginosa rhlAB genes encoding a rhamnosyltransferase involved in rhamnolipid biosurfactant synthesis. J Biol Chem. 1994; 269: 19787–95. [PubMed: 8051059]
31. de Kievit T, Seed PC, Nezezon J, Passador L, Iglewski BH. RsaL, a novel repressor of virulence gene expression in Pseudomonas aeruginosa. J Bacteriol. 1999; 181: 2175–84. [PubMed: 10094696]
32. Rampioni G, Bertani I, Zennaro E, Polticelli F, Venturi V, Leoni L. The quorum-sensing negative regulator RsaL of Pseudomonas aeruginosa binds to the lasI promoter. J Bacteriol. 2006; 188: 815–9. [PubMed: 16385073]
33. Tremblay J, Richardson AP, Lepine F, Deziel E. Self-produced extracellular stimuli modulate the Pseudomonas aeruginosa swarming motility behaviour. Environ Microbiol. 2007; 9: 2622–30. [PubMed: 17803784]
34. Kearns DB. A field guide to bacterial swarming motility. Nat Rev Microbiol. 2010; 8: 634–44. [PubMed: 20694026]
35. Wadhwa N, Berg HC. Bacterial motility: machinery and mechanisms. Nat Rev Microbiol. 2022; 20: 161–173. [PubMed: 34548639]
36. Caiazza NC, Shanks RM, O'Toole GA. Rhamnolipids modulate swarming motility patterns of Pseudomonas aeruginosa. J Bacteriol. 2005; 187: 7351–61. [PubMed: 16237018]
37. Santamaria G, Liao C, Lindberg C, Chen Y, Wang Z, Rhee K, Pinto FR, Yan J, Xavier JB. Evolution and regulation of microbial secondary metabolism. Elife. 2022; 11
38. Deng P, de Vargas RL, van Ditmarsch D, Xavier JB. The ecological basis of morphogenesis: branching patterns in swarming colonies of bacteria. New J Phys. 2014; 16: 015006–15006.
39. Gude S, Pince E, Taute KM, Seinen AB, Shimizu TS, Tans SJ. Bacterial coexistence driven by motility and spatial competition. Nature. 2020; 578: 588–592. [PubMed: 32076271]
40. Celedón RS, Díaz LB. Natural Pigments of Bacterial Origin and Their Possible Biomedical Applications. Microorganisms. 2021; 9: 739. [PubMed: 33916299]
41. Luo N, Wang S, Lu J, Ouyang X, You L. Collective colony growth is optimized by branching pattern formation in Pseudomonas aeruginosa. Mol Syst Biol. 2021; 17 e10089 [PubMed: 33900031]
42. Huberman BA, Glance NS. Evolutionary games and computer simulations. Proc Natl Acad Sci U S A. 1993; 90: 7716–8. [PubMed: 8356075]
43. Nowak MA, Sigmund K. The Alternating Prisoner's Dilemma. Journal of Theoretical Biology. 1994; 168: 219–226.

44. Ohtsuki H, Hauert C, Lieberman E, Nowak MA. A simple rule for the evolution of cooperation on graphs and social networks. Nature. 2006; 441: 502–5. [PubMed: 16724065]
45. Lieberman E, Hauert C, Nowak MA. Evolutionary dynamics on graphs. Nature. 2005; 433: 312–6. [PubMed: 15662424]
46. Darch SE, West SA, Winzer K, Diggle SP. Density-dependent fitness benefits in quorum-sensing bacterial populations. Proc Natl Acad Sci U S A. 2012; 109: 8259–63. [PubMed: 22566647]
47. Denervaud V, TuQuoc P, Blanc D, Favre-Bonte S, Krishnapillai V, Reimmann C, Haas D, van Delden C. Characterization of cell-to-cell signaling-deficient Pseudomonas aeruginosa strains colonizing intubated patients. J Clin Microbiol. 2004; 42: 554–62. [PubMed: 14766816]
48. Schaber JA, Carty NL, McDonald NA, Graham ED, Cheluvappa R, Griswold JA, Hamood AN. Analysis of quorum sensing-deficient clinical isolates of Pseudomonas aeruginosa. J Med Microbiol. 2004; 53: 841–853. [PubMed: 15314190]
49. Andersen SB, Ghoul M, Marvig RL, Lee ZB, Molin S, Johansen HK, Griffin AS. Privatisation rescues function following loss of cooperation. Elife. 2018; 7
50. Jin Z, Li J, Ni L, Zhang R, Xia A, Jin F. Conditional privatization of a public siderophore enables Pseudomonas aeruginosa to resist cheater invasion. Nat Commun. 2018; 9 1383 [PubMed: 29643375]
51. Steenackers HP, Parijs I, Dubey A, Foster KR, Vanderleyden J. Experimental evolution in biofilm populations. FEMS Microbiol Rev. 2016; 40: 373–97. [PubMed: 26895713]
52. Vega NM, Gore J. Collective antibiotic resistance: mechanisms and implications. Curr Opin Microbiol. 2014; 21: 28–34. [PubMed: 25271119]
53. Muok AR, Briegel A. Intermicrobial Hitchhiking: How Nonmotile Microbes Leverage Communal Motility. Trends Microbiol. 2021; 29: 542–550. [PubMed: 33160853]

Europe PMC Funders Author Manuscripts

Editor summary

Experimental evolution experiments show that a microbial population is more vulnerable to invading cheaters in a spatially extended system due to a higher level of cooperation.

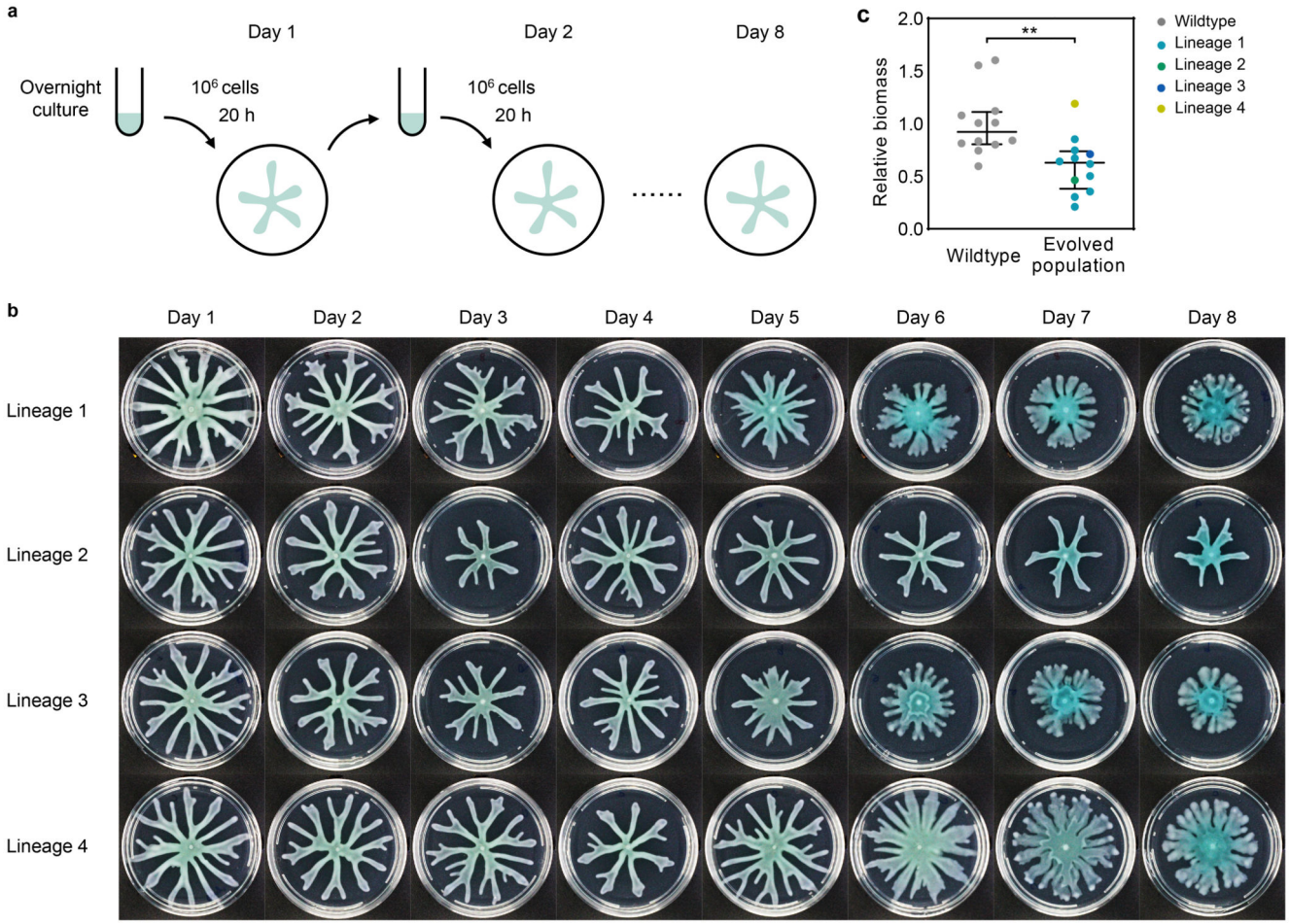

Figure 1. Experimental evolution of *Pseudomonas aeruginosa* led to reduced colony biomass.

a. *P. aeruginosa* PA14 (wildtype) was subjected to experimental evolution by sequential passages of growth on solid swarming medium. On each day, the entire colony was flushed off the plate, and a fraction of the population was inoculated onto a fresh plate.

b. The patterns of *P. aeruginosa* colonies gradually changed over the course of evolution.

c. The total biomass of colonies developed by evolved populations significantly reduced compared to wildtype colonies. Evolved populations (harvested on Day 7): n = 9 for lineage 1 and n = 1 for lineage 2-4; Wildtype: n = 12. The biomass was determined by measuring OD_{600} (normalized by the average of wildtype colonies). Lines indicate the median and the interquartile ranges. Unpaired, two-sided t-test with a 95% confidence interval was used to compare between groups: **P = 0.0029.

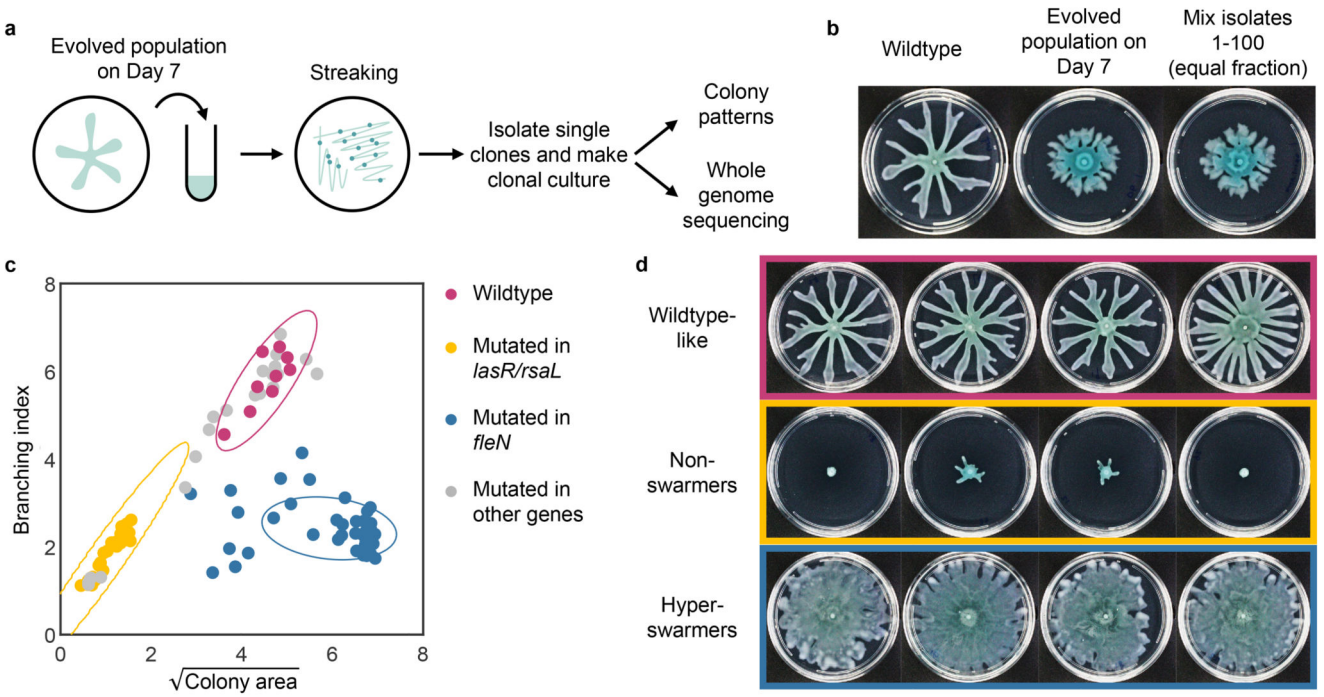

Figure 2. Phenotypic and genetic analysis identified three classes of strains in the evolved population.

a. Strains were isolated from the evolved population harvested on Day 7. We characterized colony patterns and carried out whole-genome sequencing using clonal culture of each isolate.

b. Mixing the 100 isolates with equal initial fractions reconstituted the pattern of the evolved population.

c. Phenotypes and genotypes of the isolates are closely associated. The morphology of a colony was characterized by the branching index and the colony area. Colors indicate the main types of genetic variations carried by the isolates. The probability distributions of wildtype, *lasR/rsaL* mutants, and *fleN* mutants are estimated using Gaussian KDE, and contours show the 95% confidence interval.

d. The 100 isolates fall into three categories (four of each category are shown as representatives): wildtype-like strains, nonswarmers, and hyperswarmers. The color-coding scheme (magenta for wildtype or wildtype-like strains, yellow for nonswarmers, and blue for hyperswarmers) is maintained throughout the paper.

Europe PMC Funders Author Manuscripts

Europe PMC Funders Author Manuscripts

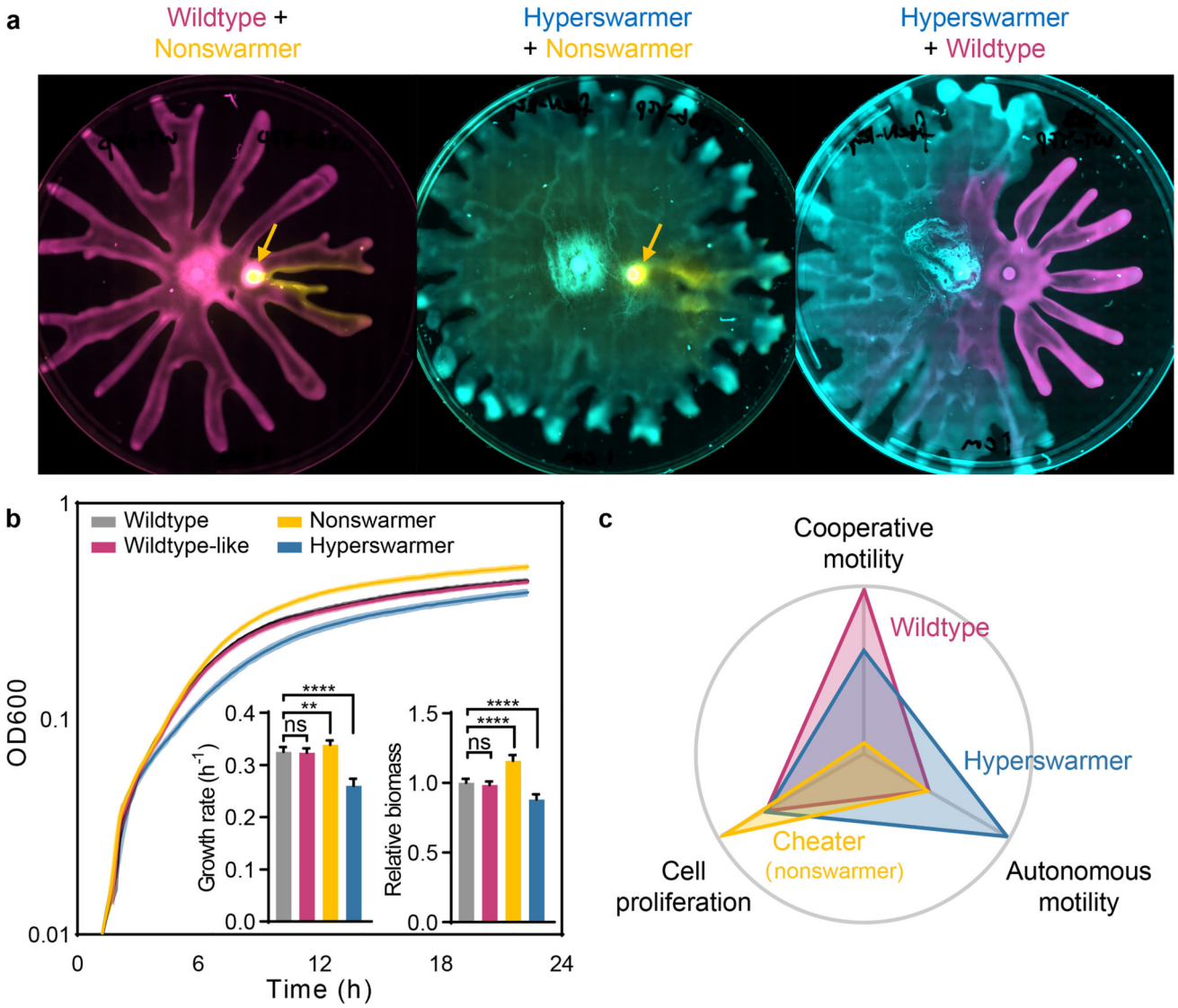

Figure 3. Wildtype, cheaters, and hyperswarmers represent different strategies of colonization.

a. Nonswarmers hitchhiked on wildtype or hyperswarmers; hyperswarmers travel faster than the others. Fluorescently labeled strains were inoculated 1 cm apart on a swarming plate and imaged after 16-18 hours of growth (see Fig. S5 for images in separate channels). Arrows indicate the locations of nonswarmer inoculums.

b. Growth rate and yield increased in nonswarmers but decreased in hyperswarmers compared to wildtype. The growth curves of wildtype (n = 12), 4 wildtype-like strains (n = 24), 3 nonswarmers (n = 17), and 4 hyperswarmers (n = 24) were shown. Thick lines show the means of the replicates, and shaded areas show SD. Insets show exponential phase growth rates and the final total biomass (normalized by wildtype) of each group, presented as mean values +/-SEM. One-way ANOVA followed by **Dunnett's multiple comparisons** test (95% confidence intervals) was used to compare between groups: **P = 0.0020; ****P < 0.0001; ns: P = 0.83 and 0.45, respectively.

c. Diagram showing the strength and weakness of each type of strains (qualitatively). Each triangle represents one type of strain. The three types of strains represent three strategies of bacteria colonization: wildtype colonize through cooperative swarming; nonswarmers (or **“cheaters”**) that grow faster and hitchhike on the swarmers; and hyperswarmers that invest more in non-cooperative, autonomous motility.

Europe PMC Funders Author Manuscripts

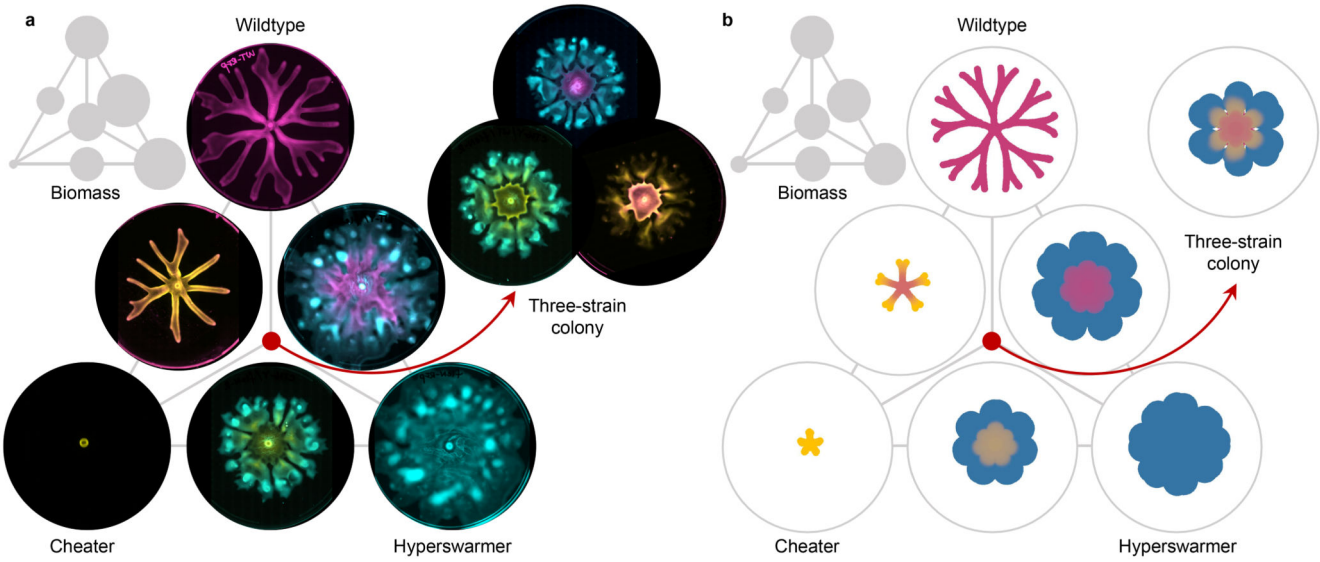

Figure 4. Constraining multi-strain colony growth model by spatial patterns.

Observed (**a**) and simulated (**b**) spatial patterns of single- or multi-strain colonies. Single- and double-strain colonies are displayed at triangle vertices and edges, respectively. Three-strain colonies (pointed out by red arrows) were fluorescently labeled with two strains at a time. Total biomass of each colony type (normalized by wildtype) is represented by circle area in the insets, mirroring the colony images' arrangement; wildtype circle sizes in **a** and **b** remain consistent. See Fig. S7 for fluorescent images in separate channels and Extended Data Fig. 5 for statistical analysis of biomass.

Europe PMC Funders Author Manuscripts

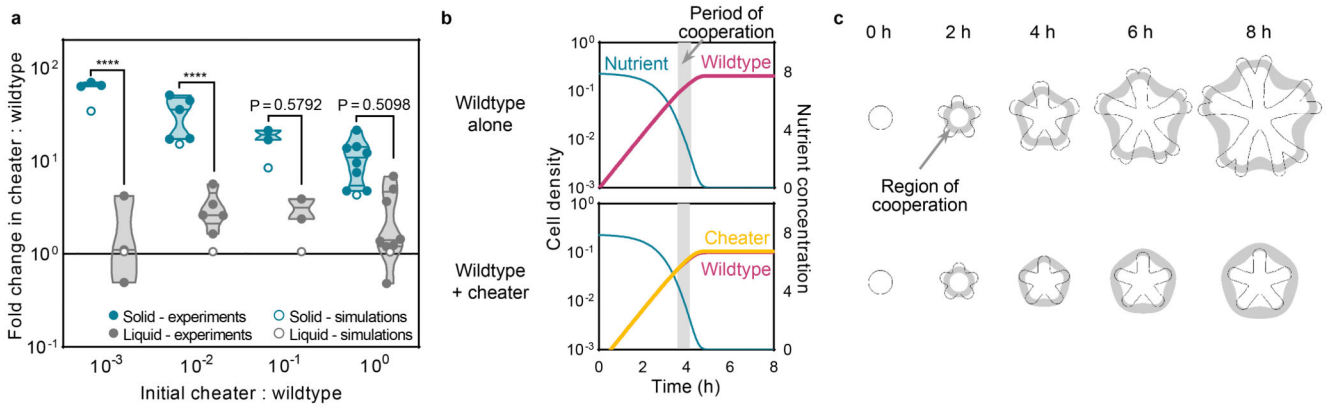

Figure 5. Increased competitive advantage of cheaters during colony expansion due to prolonged cooperation.

a. Competitive advantage of cheaters relative to wildtype was significantly higher on solid plates than in liquid media. Data points were binned by the initial cheater:wildtype ratio. For experimental data, violin plots with median and quantiles are shown; n = 3, 5, 2, and 8 when the initial cheater : wildtype = 10^{-3}, 10^{-2}, 10^{-1}, and 10^{0}, respectively. Two-way ANOVA followed by Tukey's multiple comparisons test (95% confidence intervals) was used to compare between groups: ****P < 0.0001. In simulations, identical parameters were used when comparing liquid and solid phases. The same set of data was presented in Extended Data Fig. 6a using a different format.

b, c. Simulations showed that cooperation was prolonged during colony growth (**c**) compared to liquid growth (**b**). In particular, cooperation occurred throughout the colony expansion process but occurred only briefly during liquid growth. Shaded areas in **b** and **c** represent the time window and regions, respectively, where nutrient concentration falls within the range allowing for the cooperative trait. Black thin lines show colony boundaries.

Europe PMC Funders Author Manuscripts

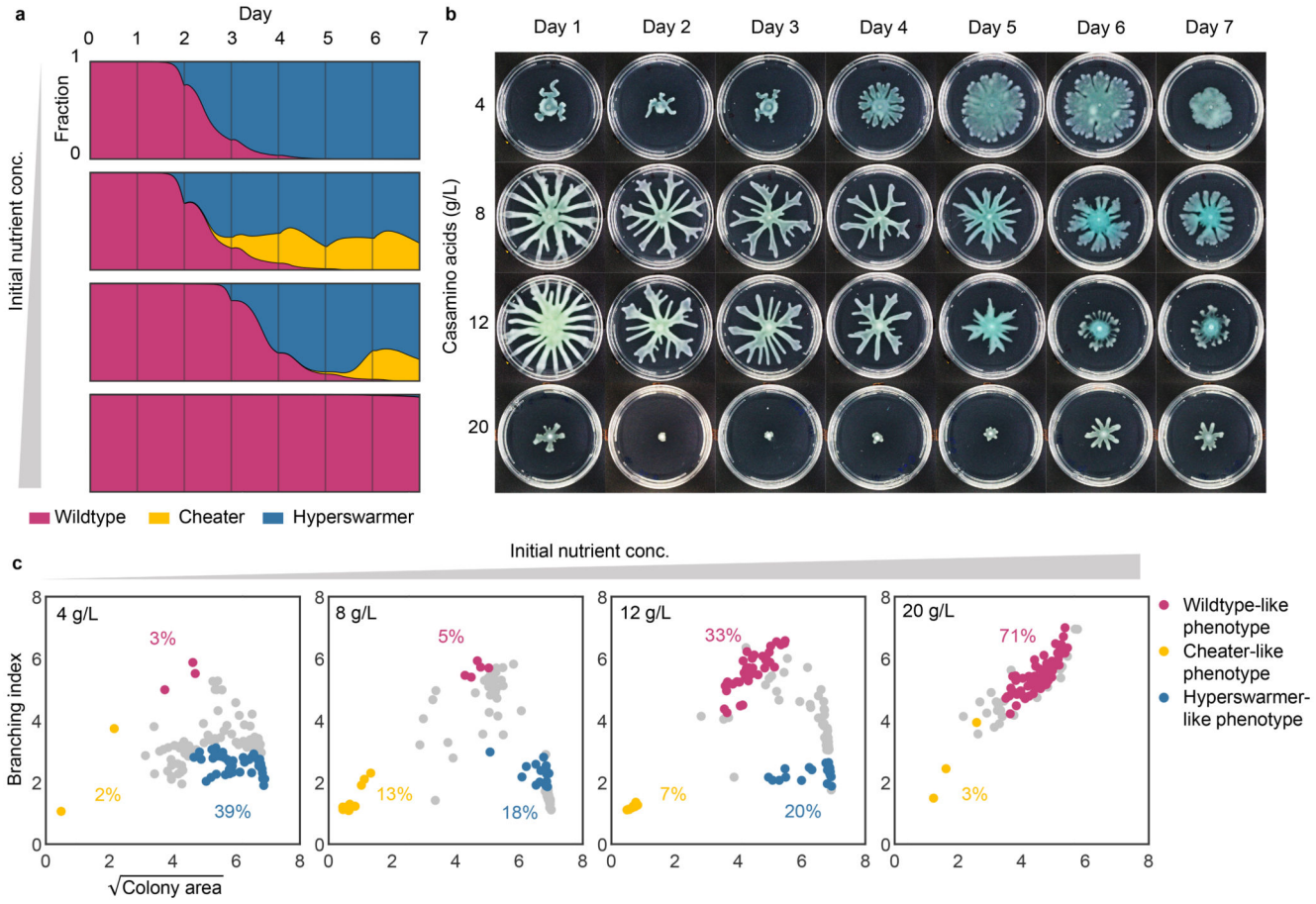

Figure 6. Evolutionary dynamics of *P. aeruginosa* colonies depended on nutrient availability.

a. Simulations showed that evolutionary outcome varies with nutrient availability. Wildtype colonies were initiated with a $1/10^7$ fraction of both cheaters and hyperswarmers. Graphs show population dynamics during cycles of colony growth and re-inoculation with an initial nutrient concentration of 0.4, 0.8, 1.2, and 1.5 (relative to the value used in Fig. 4b and Fig. 5) from top to bottom.

b. Experimental evolution of *P. aeruginosa* with different nutrient concentrations yielded different colony patterns. Three to four lineages were evolved under each condition (other lineages are shown in Fig. S11). Images in Fig. 1b (lineage 1) were reused for comparison.

c. Phenotypic analysis of isolates from the evolved populations. For each condition, data of all lineages are pooled together. The color of each data point indicates whether it falls within the 95% confidence interval of the probability distributions of each genetic group determined in Fig. 2c. Numbers indicate the percentage of isolates in each category.

Europe PMC Funders Author Manuscripts